PAPER

Ratchet effects in superconducting ring-shaped devices

IOP Publishing Superconductor Science and Technology
Supercond. Sci. Technol. 30 (2017) 105003 (7pp) https://doi.org/10.1088/1361-6668/aa821c

Ratchet effects in superconducting ring-shaped devices

Jiangdong Ji[1,2], Xingyu Jiang[2], Jie Yuan[2], Ge He[2], Biaobing Jin[1], Beiyi Zhu[2], Xiangdong Kong[3], Xiaoqing Jia[1,4], Lin Kang[1,4], Weiwei Xu[1,4], Jian Chen[1], Kui Jin[2] and Peiheng Wu[1,4]

[1] Research Institute of Superconductor Electronics (RISE), School of Electronic Science and Engineering, Nanjing University, Nanjing 210093, People's Republic of China
[2] National Laboratory for Superconductivity, Institute of Physics, Chinese Academy of Sciences, Beijing 100190, People's Republic of China
[3] Electron beam lithography technology research group, Institute of Electrical Engineering, Chinese Academy of Sciences, Beijing 100190, People's Republic of China
[4] Synergetic Innovation Center in Quantum Information and Quantum Physics, University of Science and Technology of China, Hefei, 230026, People's Republic of China

E-mail: yuanjie@iphy.ac.cn and bbjin@nju.edu.cn

Received 27 March 2017, revised 10 July 2017
Accepted for publication 25 July 2017
Published 22 August 2017

Abstract

The vortex ratchet effects in superconducting ring-shaped NbN devices are experimentally investigated. We have studied three types of samples: a narrowing eccentric circular loop, standard circular loop, and widening eccentric circular loop. Using the time-dependent Ginzburg–Landau simulations, we demonstrate that the sample edges significantly influence the dynamics of the vortices entering the samples. Through transport measurements with dc and ac currents, strong rectified voltage responses were observed for all the samples over a wide range of temperatures, critical currents, and magnetic fields. Moreover, there are some differences in the detailed ratchet behaviors among them. Furthermore, we also observed the ratchet effects in our samples caused by the current-induced field, which deserves further investigations.

Supplementary material for this article is available online

Keywords: superconducting devices, vortex motion, ratchet effects, fluxonics

(Some figures may appear in colour only in the online journal)

1. Introduction

Ratchet effects have generated increasing interest owing to their attractive characteristics in governing the transport of tiny particles, thereby facilitating the realization of many novel electronic and molecular devices in a wide range of fields [1–6]. Vortex ratchet effect, which controls the motion of flux quanta, can contribute to many applications, particularly in removing undesirable vortices in superconducting devices and upgrading their performance. Several different ideas to control the vortex motion by ratchet potentials have been proposed theoretically and realized experimentally in a variety of systems [7–18].

Compared with the vortex ratchet effects in superconductors with periodic asymmetric pinning potential arrays, which are widely studied in conventional ratchet systems [7–12], the ratchet vortex behaviors based on asymmetric edges or sharp turns of the superconductors show clear advantages, because they can provide strong ratchet response over a relatively broad range of external parameters, such as temperature and magnetic field [13–18]. These types of geometries often make it easier for vortices to enter and exit through one side of the superconductor than the other. Moreover, they are common in a variety of superconducting bridges, circuits, and devices, such as hot-electron bolometer mixers, superconducting single photon detectors,

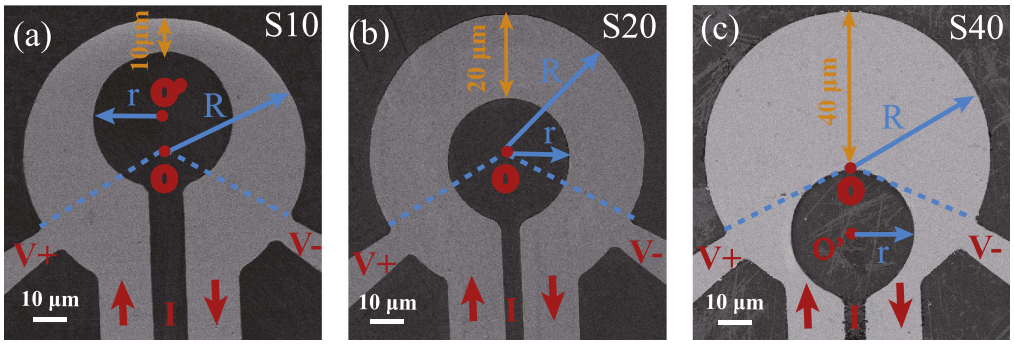

Figure 1. SEM micrographs of the three samples: (a) S10, (b) S20, and (c) S40. The geometrical parameters are $R = 40\ \mu$m, $r = 20\ \mu$m, and NbN film thickness $d = 100$ nm. (R and r are the outer and inner radii of curvature in the sample, respectively.) The angle between the two voltage contacts is 240°. The smallest width of S10 is 10 μm, the constant width S20 is 20 μm, and the largest width of S40 is 40 μm.

and superconducting quantum interference devices [19–23]. Thus, it is crucial to study the vortex motions in such structures and their potential impact on the performance and reliability of devices.

In [18], we experimentally observed pronounced ratchet effects in a superconducting asymmetric ring-shaped device, where the asymmetric edges create the ratchet potential, and the ratchet effect is mainly caused by the collective behavior of vortices. In this work, we further investigate the ratchet vortex motions in three different superconducting ring-shaped structures in detail. Using the time-dependent Ginzburg–Landau (TDGL) simulations, we describe the vortex dynamics in these systems. Through transport measurement with dc and ac currents, a ratchet response was observed whose strength can be tuned using ac (or dc) current amplitude, magnetic field, and temperature. The experimental and simulation results suggest the influence of the ring-shaped geometry on vortex motion in a variety of superconducting bridges and circuits.

2. Experimental details

Our samples were made of 100 nm thick NbN films, wherein the thin films were first deposited on the MgO(100) substrates using RF magnetron sputtering and were subsequently patterned using standard ultra-violet lithography followed by reactive ion etching. Three types of devices were investigated: the first one is a narrowing eccentric circular loop with the smallest width $w = 10\ \mu$m (figure 1(a)), the second one is a standard circular loop with the constant width $w = 20\ \mu$m (figure 1(b)), and the third one is a widening eccentric circular loop with the largest width $w = 40\ \mu$m (figure 1(c)); we refer to them as S10, S20 and S40, respectively. As shown by the scanning electron microscopy images in figure 1, all the microbridges were designed with two voltage contacts and two current leads. In order to ensure the accuracy of the measurements and produce a better comparison between different devices, they were fabricated with the same smooth film. The detailed dimensions of the samples are illustrated in figure 1.

The NbN films are characterized by a coherence length $\xi(0) < 5$ nm and a penetration depth $\lambda(0) > 200$ nm, which show typical type-II superconducting properties [24, 25]. As

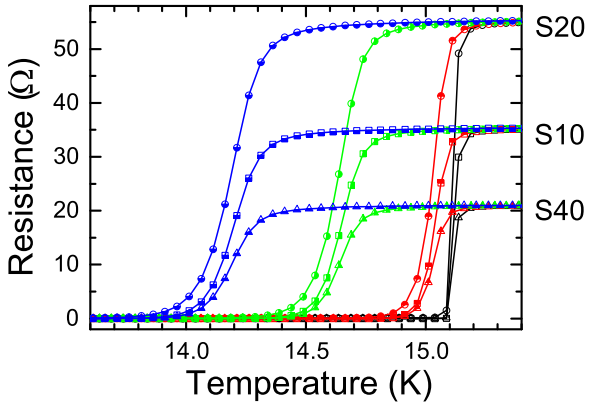

Figure 2. Temperature dependence of resistance at various external magnetic fields for the three samples. Black, red, green, and blue symbols correspond to the fields $H = 0$ T, 0.1 T, 0.5 T and 1 T, respectively.

shown in figure 2, the normal-state resistance of S20 is much larger than those of S10 and S40, whereas the normal-state resistance of S10 is larger than that of S40. This is due to the fact that to some extent, the effective cross-sectional areas of the structures of S10 and S40 increase to accommodate the current flows, leading to an increased average cross-sectional area for the sample as a whole and a reduced normal-state resistance. We define the critical temperature $T_c(H)$ using a 10% resistance criterion. The zero-field critical temperatures T_{c0} of the three samples are ~15.1 K. With an increase in the magnetic field, there are no obvious differences in the critical temperatures among these three samples. The resistance transitions for all of them are very sharp, with a typical width of ~0.1 K for $H = 0$ T and ~0.5 K for $H = 1$ T.

The transport measurements of ratchet effects were carried out using a physical properties measurement system (Quantum Design, PPMS). A current source (Keithley 6221) was used to provide both dc and ac currents, and a digital nanovoltmeter (Keithley 2182a) was used to measure the dc voltage response. The currents flowed in a clockwise manner along the microbridge as shown in figure 1, and the applied magnetic fields were always perpendicular to the sample plane.

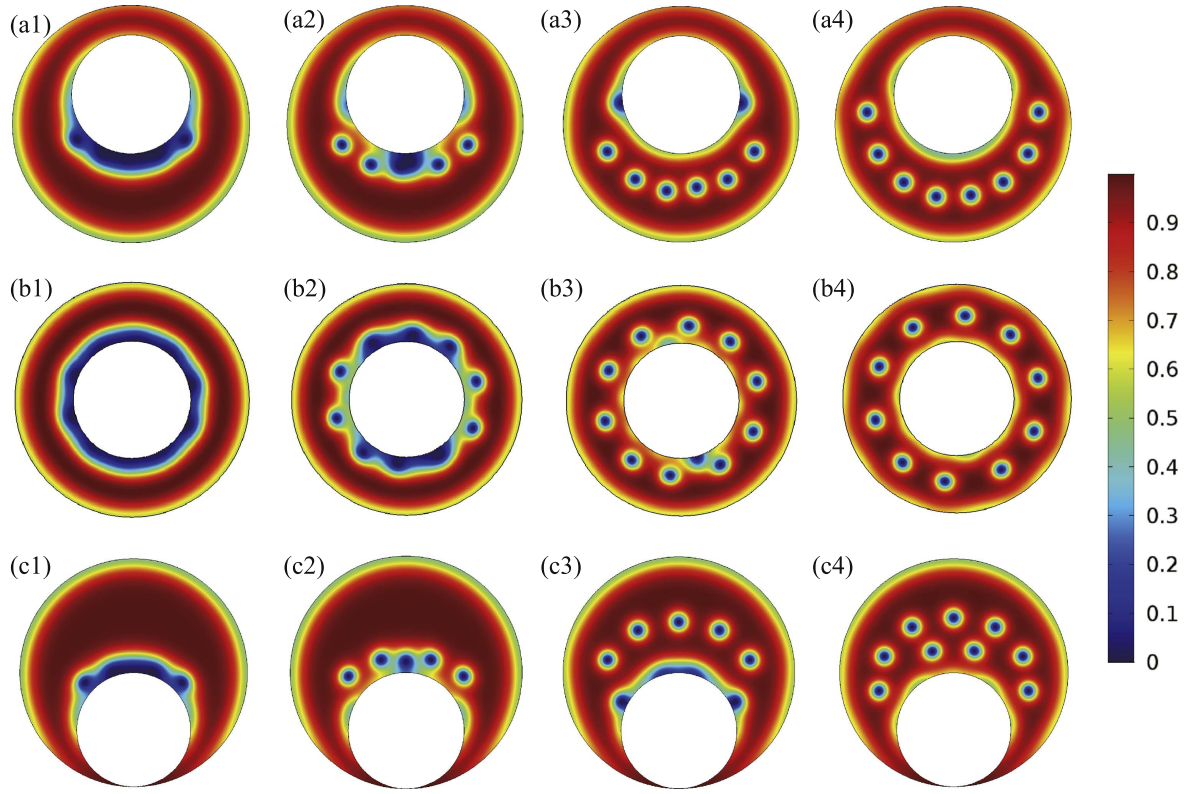

Figure 3. Time evolution of vortex motions in three sample structures. (a1)–(a4), (b1)–(b4), and (c1)–(c4) are the snapshots of the order parameter $|\psi|^2$ for S10, S20, and S40 at different times: (a1) 30, (a2) 35, (a3) 60, and (a4) 100; (b1) 50, (b2) 55, (b3) 60, and (b4) 80; (c1) 25, (c2) 30, (c3) 100, and (c4) 120. The applied magnetic field is $H = 0.4H_{c2}$. The geometrical parameters are $R = 20\xi$, $r = 10\xi$. (R and r are the outer and inner radii of curvature in the sample, respectively.) The smallest width of S10 is 5ξ, the constant width of S20 is 10ξ, and the largest width of S40 is 20ξ.

3. Results and discussions

To understand the mechanism of vortex ratchets in our devices, we performed simulations using TDGL equations. This simulation primarily reflects the entrance/nucleation and arrangement of Abrikosov vortices under the influence of sample edges in the presence of a uniform perpendicular magnetic field H. Thus, for the sake of simplicity, we consider three different superconducting circular-ring models regardless of the applied currents. As shown in figure 3, the shapes of the simulation models, despite being relatively smaller in scale, nevertheless share the same form as our samples. In the simulation models, all the regions are connected, and we are only probing the dynamics of vortices in the regions corresponding to our samples. Simulations are performed with the Ginzburg–Landau parameter $\kappa = 2$, and the normal-state conductivity $\sigma = 1$. Time is in units of $\tau = \xi^2/D$, where D is the diffusion coefficient.

The time evolution of vortices penetrating into the three samples is illustrated in figure 3. We observed that, under the applied field of $H = 0.4H_{c2}$ for all the three samples, only the inner edges of the samples could facilitate nucleation of vortices and their entry into the superconductor. Thus, a clear lower entrance barrier for vortices could be observed at the inner side of the ring-shaped devices. Predictably, by applying a driving force, this observed asymmetry could produce easy and hard directions for vortex motions, thereby leading to ratchet potentials and rectification vortex motions. With an increase in the magnetic fields, the vortices could penetrate the samples from both the inner and outer edges, which will weaken the ratchet potential.

Moreover, in the case of S10, the asymmetry of vortex motions mainly occurs in the wider regions when $H = 0.4H_{c2}$. In order to enable the vortices to enter the region of the narrow constriction in the middle, we should apply a higher magnetic field (more than $0.57H_{c2}$), which will also lead to higher critical magnetic field and higher critical current. Accordingly, the asymmetry mainly occurs in the thinner region. In the case of S20, the presence of vortex ratchets is distributed in nearly all the regions of the sample. In the case of S40, more vortex rows could enter and arrange more complexly within the sample in the region of the wider width, thereby resulting in strong vortex–vortex interactions.

Notably, our simulation results clearly demonstrate that the presence of asymmetric edges could influence vortex motions, which will result in the vortex ratchet effect when applying the ac driving force. However, despite the existing asymmetry, it is different from the experimental results, because current, voltage contacts and current leads were not considered in our simulations.

In figure 4(a), we present the current–voltage characteristics $V(I)$ for the three samples with an increase in the applied dc current flowing in the positive and negative directions at a temperature $T = 14$ K and a magnetic field $H = 0.1$ T. In

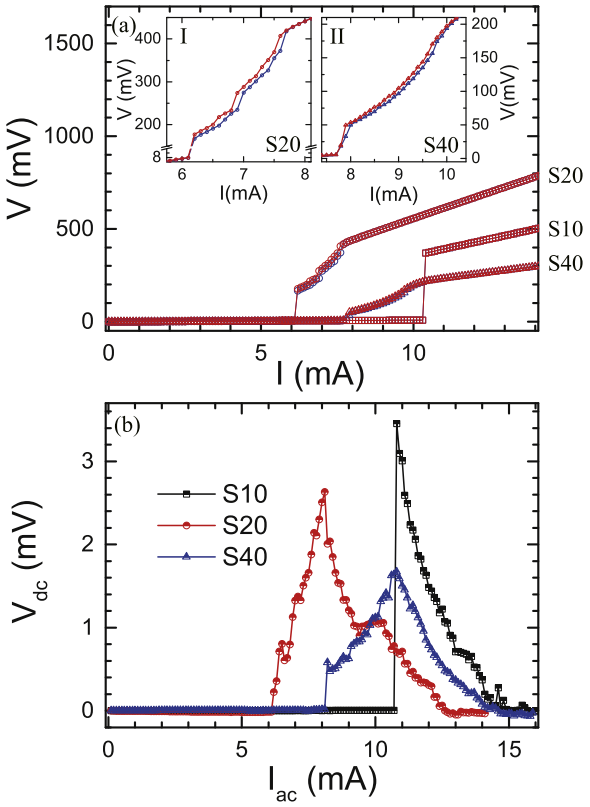

Figure 4. (a) Current–voltage characteristics for S10 (square), S20 (circle), and S40 (triangle). Blue and red symbols correspond to $V(I_+)$ and $|V(I_-)|$ respectively. Insets I and II show the asymmetries of the current–voltage characteristics in more detail for S20 and S40. (b) DC voltage as a function of ac amplitude $V_{dc}(I_{ac})$ for S10 (black square), S20 (red circle), and S40 (blue triangle) at a frequency of $f = 1k$ Hz. The temperature is $T = 14$ K, and the magnetic field is $H = 0.1$ T.

order to compare these two curves efficiently, we plot $|V(I_-)|$ instead of $V(I_-)$. The $V(I)$ curves of S20 and S40 have similar behaviors, which show several steps and jumps in the transition from the zero resistance state to the normal state. The steps and jumps in the $V(I)$ curves may result from local defects in the samples or the different vortex motions [26, 27]. However, with an increase in the current, the $V(I)$ curves of S10 transit steeply from the zero resistance state to the normal state. This is due to the fact that the smallest width in the case of S10 makes it difficult for the vortex to penetrate the sample; therefore, the moving vortex phase in $V(I)$ curves will be suppressed apparently [27]. Therefore, the critical current of S10 is also higher, which is in agreement with our simulation results.

By applying the dc current in the opposite direction, it is observed that for all the three samples, there is no clear difference between the critical currents I_c+ and I_c-. However, in the case of S20 and S40, the spacing between $V(I_+)$ and $|V(I_-)|$ exists distinctly in the region of voltage steps (Insets I and II of figure 4), where the asymmetries of the current–voltage characteristics demonstrate apparent vortex ratchet effects.

Figure 4(b) indicates the dc voltage versus ac current amplitude characteristics $V_{dc}(I_{ac})$ with a sinusoidal current (The frequency $f = 1k$ Hz). In the case of S20 and S40, V_{dc} first rises monotonically from zero to a maximum value and thereafter decays, whereas the dc voltage signal of S10 jumps sharply to the maximum value and subsequently decays to zero. This trend is similar to the results of the $V(I)$ curves. We refer to the current region where the driving force is between the weak and strong values of the pinning force as the rectification window. The ac rectification windows of S20 and S40 are similar, whereas that of S10 is lower. We can observe that the dc rectification window is much sharper than the ac rectification window, and their shapes are not similar. This can be attributed to the regime of the measurements. Compared with applying a sinusoidal current, the measurement with dc current is equivalent to applying a square-wave pulse drive to the sample, which is similar to the results and explanations in [10].

We further investigated the temperature and magnetic field dependences of the ratchet effects in our samples. In the case of both S20 and S40, the enhancements of the ratchet signals and rectification window are observed at lower temperatures. Figure 5(a) shows the $V_{dc}(I_{ac})$ at different temperatures for S20. We observe that with the constant magnetic field ($H = 0.1$ T), when temperature decreases from T_c, the maximum dc voltage increases from ∼0.9 to ∼4.2 mV and the width of the rectification window increases from ∼4 to ∼11 mA.

In order to compare with the results for S40 (as shown in figure 4(a) of [18]), we plot the temperature dependence of the maximum V_{dc} and the ac current input I_{ac} achieved for two samples (figure 5(b)). Notably, when decreasing temperature from T_c, the maximum dc voltage increases first rapidly and thereafter slowly, whereas the ac current amplitude where the maximum V_{dc} is achieved (max I_{ac}) shifts toward higher values. At each temperature, the ac amplitude I_{ac} where the initial nonzero V_{dc} increases and the maximum I_{ac} of S20 are smaller than those of S40, which corresponds to their temperature dependences of the critical currents. However, the rectification windows and the maximum V_{dc} of S20 are larger than those of S40. We believe that it results from stronger vortex–vortex interactions and more complex vortex arrangement in S40. With an increase in the magnetic field, the ratchet voltage signal will be weakened, which also indicates that $H = 0.1$ T is closer to the optimized magnetic field for rectified vortex motions in our devices (figure 5(c)).

In S10, when the magnetic field $H = 0.1$ T, the rectified dc voltages are only observed at the temperatures of 13.5, 14 and 14.5 K, and the ratchet signals weaken clearly when $T = 13.5$ K; whereas at $T = 13$ K, we could observe the ratchet signal when applied fields are increased to $H = 0.5$ and 1 T (figure 5(d)). Further, at $H = 1$ T, the strength of the dc voltage would weaken clearly. Therefore, the ratchet behavior of S10 occurs in a narrower temperature range as compared to the other two samples, and at lower temperatures, the effective ratchet potential of S10 is strongly suppressed.

The vortex rectification in our devices is strongly dependent on temperatures and magnetic fields, which is consistent with the behavior in most other vortex ratchet

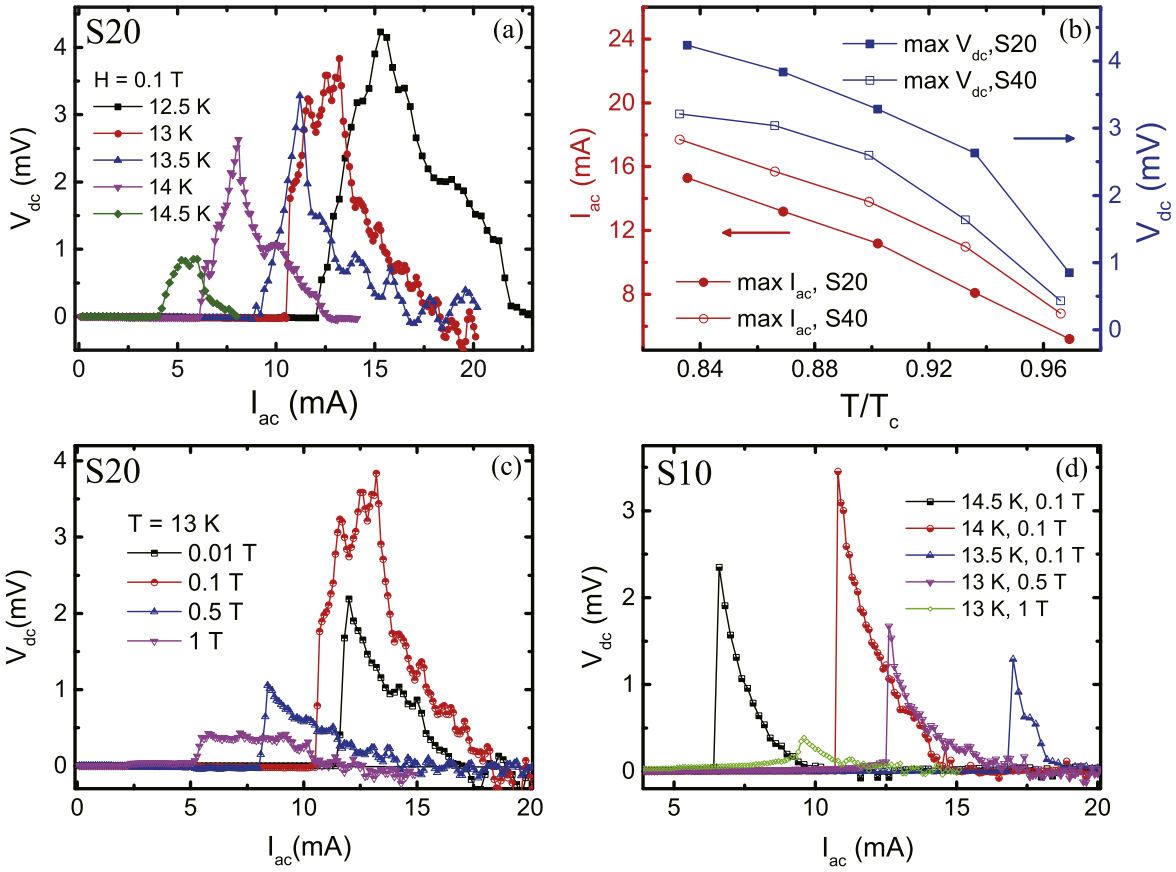

Figure 5. (a) V_{dc} as a function of ac amplitude I_{ac} for S20 at different temperatures $T = 12$, 12.5, 13, 13.5 and 14 K. The applied magnetic field is $H = 0.1$ T. (b) Temperature-dependent plot of the maximum V_{dc} and the ac current input I_{ac} achieved for S20 (solid symbols) and S40 (hollow symbols). (c) For temperature $T = 13$ K, $V_{dc}(I_{ac})$ curves for S20 at different magnetic fields $H = 0.01$, 0.1, 0.5 and 1 T. (d) $V_{dc}(I_{ac})$ curves of S10 at different temperatures and magnetic fields.

systems. The temperature dependence of the rectified voltage indicates that the vortex size and thermal fluctuation play important roles in the ratcheting process. Moreover, as our simulation results indicate, a stronger magnetic field will weaken the ratchet potentials caused by the edges of our devices. In general, strong enhancements in the rectified voltages could be observed over a wide range of temperature and magnetic field in our devices.

As shown in figure 6, we could also observe the ratchet effects in S20 and S40 samples when the applied field $H = 0$ T. The apparent rectified voltage responses are observed in $V(I)$ and $V_{dc}(I_{ac})$ curves for both the samples. Similar to the experimental results at the magnetic field $H = 0.1$ T, the ratchet effects occur above the initial critical current I_{c0} and mainly in the moving vortex state where voltage steps are observed. Regarding $V_{dc}(I_{ac})$ characteristics, the maximum V_{dc} for S20 and S40 are ~0.5 mV and ~0.12 mV, respectively. These ratchet responses are also very pronounced, which probably result from the current-induced field. Simultaneously, there might be some very low remainder fields from the PPMS or fields as small as the Earth's magnetic field. However, this indicates that our ratchet devices are extremely sensitive to external ultra-low fields, and it is worth further exploring the ratchet behaviors for these samples in the absolute absence of external magnetic fields. We did not observe clear ratchet signals at $H = 0$ T in the case of S10. It is difficult for the vortex to penetrate narrow samples with very low magnetic fields, which is consistent with our simulation results.

We have also repeated the measurements for the two samples with ac currents at various frequencies in the range from $0.1k$ Hz to $100k$ Hz. No significant changes in the results could be observed, which indicates that our ratchet devices were operated in the adiabatic regime, and according to our calculations in [18], to observe nonadiabatic ratcheting features and the frequency dependence of ratchet effects in this system, the external current frequency can be higher than several megahertz.

4. Conclusions

In conclusion, we experimentally investigated the ratchet behaviors in microscopic NbN superconducting ring-shaped devices. We demonstrated that a standard circular loop structure (S20), widening eccentric circular loop structure (S40), and narrowing eccentric circular loop structure (S10) can all provide strong vortex ratchet effects in a relatively broad range of external parameters such as temperature, current, and magnetic field. Our simulations show that the

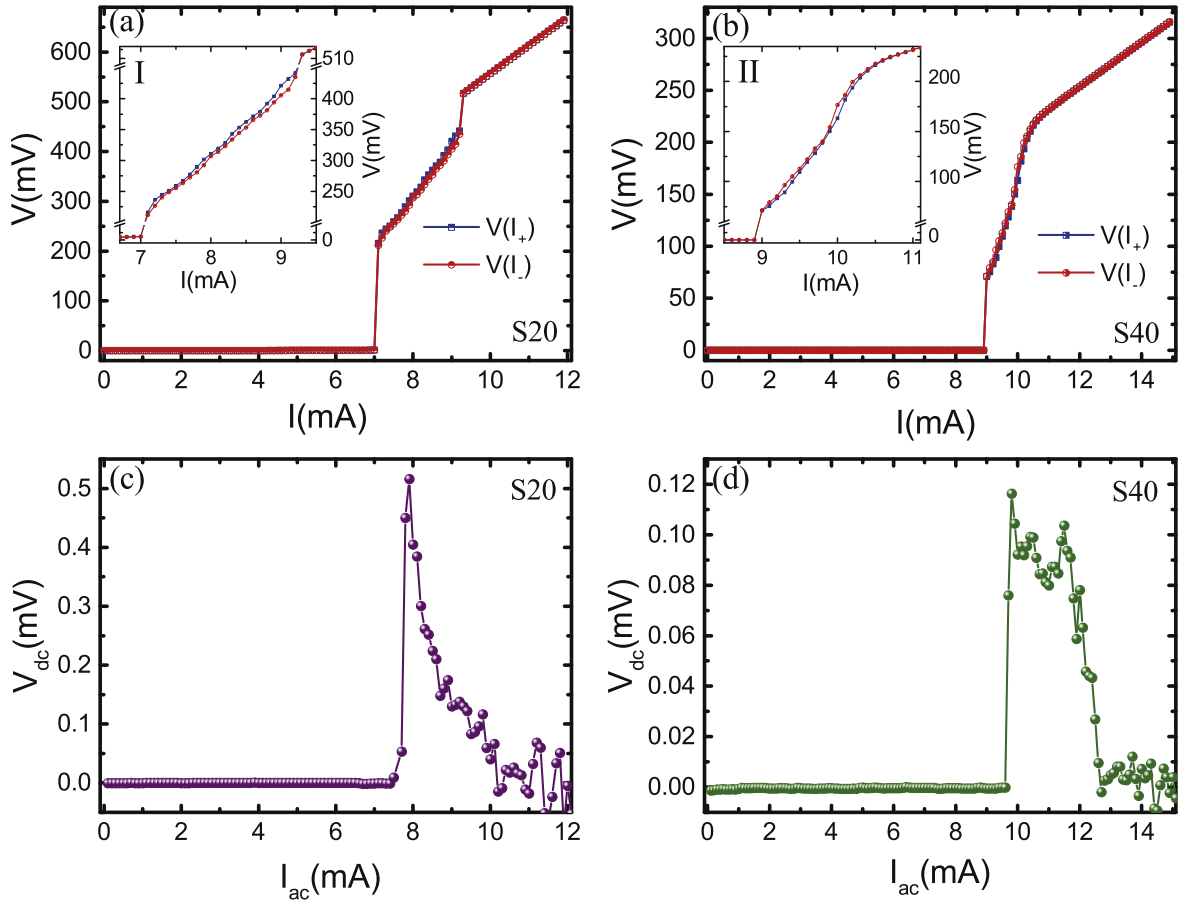

Figure 6. Current–voltage characteristics for (a) S20 and (b) S40 at the applied magnetic field $H = 0$ T. Blue and red symbols correspond to $V(I_+)$ and $|V(I_-)|$, respectively. Insets I and II show the asymmetries of the current–voltage characteristics in more detail for both samples. DC voltage as a function of ac amplitude $V_{dc}(I_{ac})$ for (c) S20 and (d) S40 at a frequency of $f = 1k$ Hz. The temperature is $T = 14$ K.

sample edges significantly influence the dynamics of the vortices entering superconductors and thereby the vortex ratchet effects. In the case of both $V(I)$ and $V_{dc}(I_{ac})$ characteristics, the ratchet features of the three samples exhibit strong dependences on temperatures and magnetic fields. In particular, rectified dc voltages were observed when the external magnetic field approached zero in S20 and S40, which may be caused by the current-induced field and is of interest for further investigations.

Acknowledgments

This work was supported by the MOST973 (Grant Nos. 2014CB339800, 2015CB921000 and 2016YFA0300301), the National Instrumentation Program (Grant No. 2012YQ140005), the National Natural Science Foundation (Grant Nos. 61671234, 61371035, 11173015, 11227904, 61521001, 6167010375, 61501219, 11674374 and 11474338), the Priority Academic Program Development of Jiangsu Higher Education Institutions, and the Jiangsu Provincial Key Laboratory of the Advanced Manipulation of Electromagnetic Wave. B B Jin also acknowledges support from the Cooperative Innovation Centre of Terahertz Science, University of Electronic Science and Technology, Chengdu, China.

ORCID iDs

Jian Chen https://orcid.org/0000-0002-1360-8969

References

[1] Feynman R P, Leighton R B and Sands M 1966 *The Feynman Lectures on Physics* (Reading, MA: Addison-Wesley) ch 46
[2] Hänggi P and Marchesoni F 2009 *Rev. Mod. Phys.* **81** 387
[3] Serreli V, Lee C F, Kay E R and Leigh D A 2007 *Nature* **445** 523
[4] Mahmud G, Campbell C J, Bishop K J M, Komarova Y A, Chaga O, Soh S, Huda S, Kandere-Grzybowska K and Grzybowski B A 2009 *Nat. Phys.* **5** 606
[5] Fujiwara A, Nishiguchi K and Ono Y 2008 *Appl. Phys. Lett.* **92** 042102
[6] Sterck A, Koelle D and Kleiner R 2009 *Phys. Rev. Lett.* **103** 047001
[7] Lee C S, Jankó B, Derényi I and Barabási A L 1999 *Nature* **400** 337
[8] Villegas J E, Savel'ev S, Nori F, Gonzalez E M, Anguita J V, Garćia R and Vicent J L 2003 *Science* **302** 1188
[9] Zhu B Y, Marchesoni F and Nori F 2004 *Phys. Rev. Lett.* **92** 180602
[10] Van de Vondel J, de Souza Silva C C, Zhu B Y, Morelle M and Moshchalkov V V 2005 *Phys. Rev. Lett.* **94** 057003

[11] Togawa Y, Harada K, Akashi T, Kasai H, Matsuda T, Nori F, Maeda A and Tonomura A 2005 *Phys. Rev. Lett.* **95** 087002
[12] Palau A, Monton C, Rouco V, Obradors X and Puig T 2012 *Phys. Rev.* B **85** 012502
[13] Adami O-A *et al* 2013 *Appl. Phys. Lett.* **102** 052603
[14] Vodolazov D Y and Peeters F M 2005 *Phys. Rev.* B **72** 172508
[15] Schildermans N, Kolton A B, Salenbien R, Marconi V I, Silhanek A V and Moshchalkov V V 2007 *Phys. Rev.* B **76** 224501
[16] Cerbu D, Gladilin V N, Cuppens J, Fritzsche J, Tempere J, Devreese J T, Moshchalkov V V, Silhanek A V and Van de Vondel J 2013 *New J. Phys.* **15** 063022
[17] Harrington S A, MacManus-Driscoll J L and Durrell J H 2009 *Appl. Phys. Lett.* **95** 022518
[18] Ji J D, Yuan J, He G, Jin B B, Zhu B Y, Kong X D, Jia X Q, Kang L, Jin K and Wu P H 2016 *Appl. Phys. Lett.* **109** 242601
[19] Hortensius H L, Driessen E F C, Klapwijk T M, Berggren K K and Clem J R 2012 *Appl. Phys. Lett.* **100** 182602
[20] Halbertal D *et al* 2016 *Nature* **539** 407
[21] Day P K, LeDuc H G, Mazin B A, Vayonakis A and Zmuidzinas J 2003 *Nature* **425** 817
[22] Mittendorff M, Winnerl S, Kamann J, Eroms J, Weiss D, Schneider H and Helm M 2013 *Appl. Phys. Lett.* **103** 021113
[23] Natarajan C M, Tanner M G and Hadfield R H 2012 *Supercond. Sci. Technol.* **25** 063001
[24] Kumar S, Kumar C, Jesudasan J, Bagwe V, Raychaudhuri P and Bose S 2013 *Appl. Phys. Lett.* **103** 262601
[25] Grimaldi G, Leo A, Nigro A, Silhanek A V, Verellen N, Moshchalkov V V, Milosevic M V, Casaburi A, Cristiano R and Pace S 2012 *Appl. Phys. Lett.* **100** 202601
[26] Berdiyorov G, Harrabi K, Oktasendra F, Gasmi K, Mansour A I, Maneval J P and Peeters F M 2014 *Phys. Rev.* B **90** 054506
[27] Berdiyorov G, Chao X H, Peeters F M, Wang H B, Moshchalkov V V and Zhu B Y 2012 *Phys. Rev.* B **86** 224504